KELVIN PROBE FORCE MICROSCOPY IMAGING AND CHARACTERIZATION OF ORGANIC PHOTOVOLTAICS

A Thesis
by
JOSEPH P. GODOY

Submitted to the Graduate School
at Appalachian State University
in partial fulfillment of the requirements for the degree of
MASTER OF SCIENCE

August 2021
Department of Physics and Astronomy

KELVIN PROBE FORCE MICROSCOPY IMAGING AND CHARACTERIZATION OF ORGANIC PHOTOVOLTAICS

A Thesis
by
JOSEPH P. GODOY
August 2021

APPROVED BY:

Dr. Tonya S. Coffey, PhD
Chairperson, Thesis Committee

Dr. Brooke C. Hester, PhD
Member, Thesis Committee

Dr. Francois Amet, PhD
Member, Thesis Committee

Dr. Courtney E. McGahee, PhD
Chairperson, Department of Physics and Astronomy

Dr. Michael J. McKenzie, Ph.D.
Dean of the Cratis D. Williams School of Graduate Studies

Abstract

KELVIN PROBE FORCE MICROSCOPY IMAGING AND CHARACTERIZATION OF ORGANIC PHOTOVOLTAICS

Joseph P. Godoy
B.S. Physics, High Point University
M.S. Engineering Physics, Appalachian State University

Chairperson: Dr. Tonya S. Coffey, Ph.D

Photovoltaics are semiconductors capable of transforming light incident upon their surfaces into electric currents. This property makes them a promising alternative to non-renewable energy sources. As of 2021, most commercially available photovoltaics are composed of layers of monocrystalline silicon. However, there is a growing interest in organic polymer photovoltaics (OPVs) which are thought to be more sustainable and easier to manufacture. Using kelvin probe force microscopy (KPFM), we generated nano- and micro- scale surface potential and topography images of various organic thin films to develop a better understanding of their compositions, crystallinities, and morphologies. These included various annealed and unannealed blends of phenyl-C61-butyric acid methyl ester (PCBM) and two different squaraine dyes: DBSQ(OH)2, and DHSQ(OH)2. We found the average work functions of the squaraines to be roughly the same. This implies that any KPFM contrast in blends containing only squaraines is due to local variations in crystallinity rather than compositional domains. The premise of the experiment was to test whether the

good mixing of the DBSQ:PCBM binary blends and the high charge mobility caused by the tight packing of the DHSQ:PCBM binary blends could be combined and optimized in a ternary DHSQ:DBSQ:PCBM blend. Unfortunately, we found that the middle-ground ternary blends (50:25:25 PCBM:DBSQ:DHSQ) had slightly larger domains than the DBSQ:PCBM binary blends -- which had the smallest compositional domains -- and yielded the lowest short circuit current density when tested by our collaborators at RIT. This implies that neither the good mixing of the DBSQ blends nor the high charge mobility of the DHSQ blends were present in the middle-ground 50:25:25 ternary blend.

Acknowledgments

I would like to thank my mom, who has always been there for me, and whose help I would not be here without. I offer my thanks to the members of the Committee, Dr. Francois Amet and Dr. Brooke Hester, and especially the Chairperson, Dr. Tonya S. Coffey, for their flexibility during difficult times. I would also like to thank Dr. Chris Thaxton for his statistical image analyses, Dr. Chris Collison, for his material samples, and Tyler Wiegand, for going far out of his way to provide me with useful information, resources, and figures.

Table of Contents

Background

Introduction

According to a provisional report by the World Meteorological Organization, the global mean temperature for 2020 was 1.2 ± 0.1 °C above the pre-industrial temperature baseline.[1] Ocean levels are rising and ice sheets are shrinking. It is the consensus of the World Meteorological Organization and the scientific community behind it that these adverse environmental effects have been caused by human activities. As the broad public interest in preventing climate change and promoting sustainability continues to grow, so too grows the demand for renewable energy technologies in a market primarily dominated by coal and natural gas.[2] One emerging group of renewable technologies is known as *photovoltaics*: a broad range of semiconductor devices capable of converting light incident upon their surfaces into usable energy.

The process of converting light into energy can be broken down into four key steps. First, incident light is absorbed by a semiconductor, exciting an electron from the valence band to the conduction band. This leaves behind a

[1] "State Of The Global Climate 2020: Provisional Report." World Meteorological Organization, December 2020, https://public.wmo.int/en/our-mandate/climate/wmo-statement-state-of-global-climate
[2] "Global Energy Review 2020." International Energy Association, April 30 2020, https://www.iea.org/reports/global-energy-review-2020

vacancy, often referred to as a *hole*, in the host atom, which effectively acts as a carrier of positive charge.[3] Next, the excited electrons are bound with the holes formed in their host atoms to become bound electron-hole pairs, or, *excitons*. Next, the excitons must be dissociated to prevent them from recombining before the charge carriers can be separated. Lastly, the charges are transported to opposite terminals, resulting in a potential difference which can be used to supply current to an electrical circuit between the contacts.

These devices are typically composed of one or more interfaces between *p-type* materials, which have an excess of holes, and *n-type* materials, which have an excess of electrons. This type of p-n junction interface forms the fundamental building blocks of transistors, diodes, and other useful semiconductor devices.

Significant strides have been made in the development of photovoltaic devices since the first plutonium and silver nitride-based solar cell developed by Becquerel in 1839. As of 2020, most commercially-available photovoltaic devices are clustered around twenty percent efficiency and are typically composed of junctions between phosphorus-doped and boron-doped silicon.

However, notable improvements to existing photovoltaic technologies are not limited to increases in device efficiency. A 2020 paper in *Energy Strategy Reviews* outlines many of the adverse environmental effects associated with the

[3] Myung-Su Kim, "Understanding Organic Photovoltaic Cells: Electrode, Nanostructure, Reliability, and Performance," PhD dissertation (University of Michigan, 2009): 2-3.

disposal of solar panels that have reached the end of their operating lives. At the end of 2016, there were approximately 250,000 metric tonnes of waste due to end-of-life photovoltaic devices.[4] This number is expected to increase to 9.5 million metric tonnes by the year 2050. The contents of many commercially-available thin film photovoltaics contain heavy metals such as zinc, lead, copper, indium, and chromium, which have been found to be toxic in low doses.[5] A paper in *Applied Geochemistry* describes an experiment in which thin film solar panels (TFSPs) were coated with an acid extract to simulate corrosion, and buried in soil. Within sixty days, the soil samples were evaluated, and the concentration of certain metals, such as nickel, were found to exceed the limits provided by national environmental quality standards for soil.[6]

While there are new developments in recycling processes for end-of-life TFSPs, there are also ongoing research efforts focused on exploring alternative materials for manufacturing photovoltaic devices which do not lend themselves to the same environmental hazards that current commercially-available thin film solar panels are prone to. In the next section, we will discuss one such emerging group of materials known as organic photovoltaics (OPVs).

---

[4] Chowdhury, et. al. "An Overview of Solar Photovoltaic Panels' End-of-Life Material Recycling," *Energy Strategy Reviews* (2020): 4.
[5] Bhat, et. al. "Heavy Metal Toxicity and Their Harmful Effects on Living Organisms -- A Review," *International Journal of Medical Science And Diagnosis Research* (2020): 6.
[6] Su, et. al. "Release of Metal Pollutants From Corroded and Degraded Thin-Film Solar T Panels Extracted by Acids and Buried in Soils," *Applied Geochemistry* (2019): 1.

Organic Semiconductors & Photovoltaics

Unlike their metallic counterparts, organic polymers do not typically exhibit semiconductor-like properties. In order to make an organic polymer behave as a conductor or semiconductor, the polymer molecules should first be composed of a chain of alternating single-and-double bonds, also known as *conjugated* double bonds.[7]

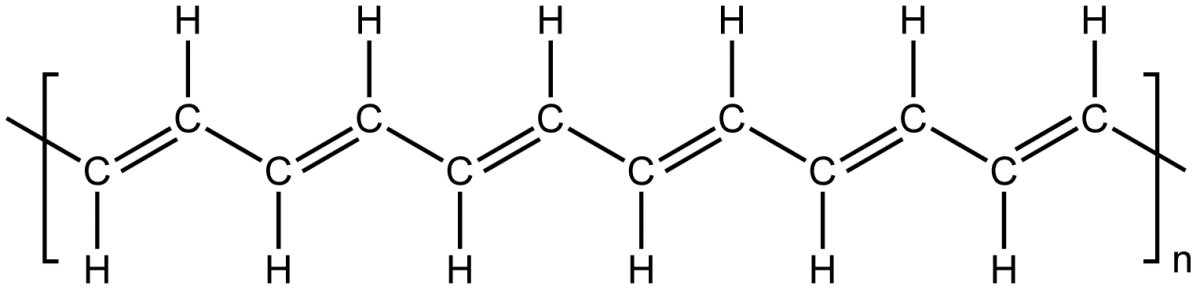

Figure 1: Conjugated double bonds in polyacetylene.[7]

Next, a dopant should be introduced to the conjugated double bond structure, either through oxidation or reduction to create an absence or excess of electrons, respectively. This allows double bonds to travel across the chain, and even hop from molecule to molecule. This charge transport mechanism was the subject of the 2000 Nobel prize in chemistry, awarded to Heeger, MacDiarmid, and Shirakawa, who discovered that the electrical conductivity of polyacetylene

[7] Smokefoot, "Trans-CH(n)," *Wikimedia Commons*, December 28 2006. https://commons.wikimedia.org/wiki/File:Trans-(CH)n.png

increased one billion-fold when oxidized with iodine vapor.[8] One consequence of an organic semiconductor's molecular structure is a wide range of possible vibrational energy states. These states and the possible transitions between them are illustrated in the Perrin-Jablonski diagram in figure 2.

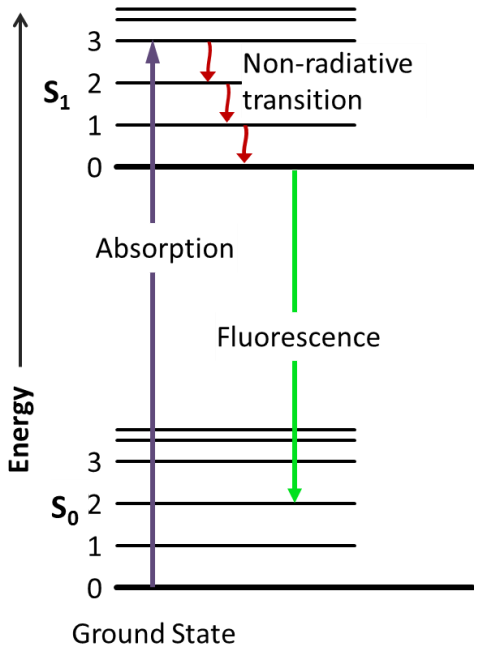

Figure 2: Fluorescence-only *Perrin-Jablonski* diagram of an organic molecule.[9]

The bold horizontal lines represent the vibrational ground state for each electronic state, and the thin horizontal lines represent the excited vibrational modes for each electronic state. Note that each vibrational state can be divided

[8] The Royal Swedish Academy of Sciences, "The 2000 Nobel Prize in Chemistry," October 10 2000. https://www.nobelprize.org/prizes/chemistry/2000/popular-information/
[9] Jacobkhed, "Jablonski diagram of absorbance, non-radiative decay, and fluorescence." *Wikimedia Commons*, April 22 2012. https://commons.wikimedia.org/wiki/File:Jablonski_Diagram_of_Fluorescence_Only.png

into many rotational sub-levels. Radiative transitions, denoted by straight arrows, are transitions in which the energy difference between two states is an absorbed or emitted photon. These transitions are preferable in photovoltaic devices, as re-emitted photons can be re-absorbed and used to create additional excitons and promote charge transfer. Non-radiative transitions, denoted by oscillating arrows, are transitions in which the energy difference between two states is not an absorbed or emitted photon. These transitions provide paths for intermolecular energy transfer, but also paths for energy to become waste heat.[11]

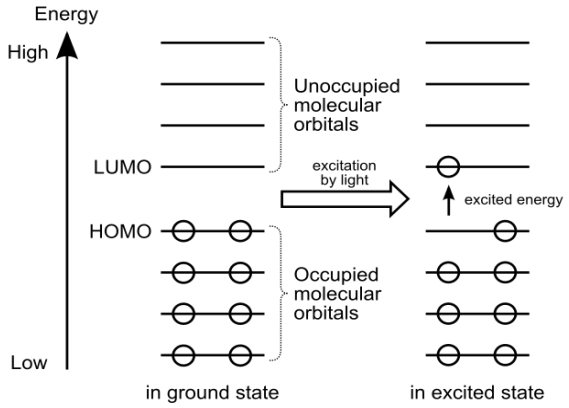

Figure 3: Simplified excitation process in a photovoltaic molecule.[10]

While it is important to consider the wide range of fluorescent and vibrational charge transfer mechanisms that take place in organic photovoltaics, the fundamental principles governing the operation of an OPV are not unlike

[10] Tomgally, "Molecule HOMO-LUMO diagram.svg." *Wikimedia Commons*, January 19 2020. https://upload.wikimedia.org/wikipedia/commons/7/7b/Molecule_HOMO-LUMO_diagram.svg

those of a conventional photovoltaic. First, incident light is absorbed by electrons in the donor molecules, resulting in the generation of an exciton. However, if the absorbed energy exceeds the band gap, the electron will be excited to an energy level above the lowest unoccupied molecular orbital (LUMO) and the energy will be lost to thermalization after decay.[11] Next, excitons must be diffused to the boundary between the donor and acceptor material. In a typical organic semiconductor, excitons will travel roughly 10 nm before the bound electron-hole pair recombine. Consequently, smaller compositional domains are typically better equipped to diffuse excitons than larger ones, as the exciton has a higher probability of making it to the donor-acceptor boundary. Once an exciton has reached the donor-acceptor boundary, it must be dissociated. The energy difference between the LUMO level of the donor and the LUMO level of the acceptor is the primary driver of exciton dissociation. Once the electron transitions to the acceptor's LUMO level, the charge carriers will form a charge transfer state, where the electron and hole experience a coulombic attraction which weakens as the distance between them increases.[11] Lastly, the charge-carriers are transported to their respective electrodes and collected, where they can be used to supply current to a load. In the next section, we will discuss candidate materials that help to facilitate this process.

[11] Spooner, Emma, "Organic Photovoltaics: An Introduction." *Ossila*. Accessed January 25 2021. https://www.ossila.com/pages/organic-photovoltaics-introduction

PCBM

When selecting organic semiconductors to act as donor and acceptor materials, practical considerations are not limited to electronic structure or power-conversion efficiency-related features. Before organic photovoltaic devices can be manufactured for commercial applications, scalable deposition and manufacturing techniques need to be developed, as well as materials which can be deposited with these methods.

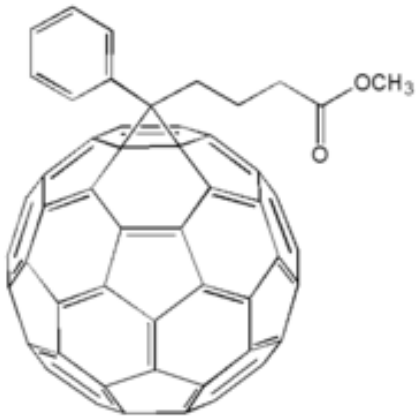

Figure 4: Phenyl-C61 butyric acid methyl ester (PCBM), a fullerene-based electron acceptor.[12]

[12] Cubane, "PCBM," *Wikimedia Commons,* November 7, 2009. https://commons.wikimedia.org/wiki/File:PCBM.png

While there have been ongoing research efforts into small non-fullerene acceptor (NFA) molecules with improved optical absorption properties, fullerene-based molecules hold the current performance benchmarks for electron acceptors in organic photovoltaic devices.[13,14] Phenyl-C61-butyric acid methyl ester (PCBM) is one such material: a fullerene derivative that acts as an electron acceptor, and can be spin-coated or vapor-deposited onto a substrate. Like other fullerene-based acceptors, PCBM has several distinct features which make it a useful compound for OPV devices. First, the degree of control over the nanoscale morphology when synthesizing PCBM-based blends is known to be favorable for exciton diffusion when blended with suitable donor materials, yielding compositional domain sizes on the same order of magnitude as the exciton recombination length.[15]

Other useful properties of PCBM include its high electron affinity, electron mobility, and three-dimensional electron transport processes.[13] In the next section, we will discuss donor materials which can be used in tandem with PCBM to create performant organic photovoltaic devices.

[13] Zheng, et. al., "Impact of Alkyl Chain Length on Small Molecule Crystallization and Nanomorphology in Squaraine-Based Solution Processed Solar Cells," *The Journal of Physical Chemistry C* 121 (2017): 7750.
[14] Yang, et. al., "A New Wide Band Gap Donor for Efficient Fullerene-Free All-Small-Molecule Organic Solar Cells," *Journal of the American Chemical Society* 139 (2017): 1958.
[15] Tao Liu and Alessandro Troisi, "What Makes Fullerene Acceptors Special as Electron Acceptors in Organic Solar Cells and How to Replace Them," *Advanced Materials* 25 (2013): 1038.

Squaraine Dyes

Squaraines are π-conjugated organic compounds derived from squaric acid. These molecules have a wide range of useful properties when used in organic photovoltaics, which often include large extinction coefficient values, relatively straightforward synthesis processes, and highly tunable molecular structures.[16] Certain squaraines, such as DBSQ(OH)2 and DHSQ(OH)2, act as electron donors and can be blended with electron acceptors, such as fullerene-based PCBM molecules, to create a relatively efficient class of organic photovoltaic devices known as dye-sensitized solar cells (DSSCs).

The mechanisms by which squaraine dyes contribute to the overall performance and power-conversion efficiency remain controversial. In a 2020 paper titled *Aggregation as an Efficiency Driver in Bulk Heterojunction Devices Measured Through Mixed Squaraines in Ternary Blends,* Gupta argues that the key property of squaraine dyes which contributes to the efficiency of dye-sensitized devices is the ability of squaraine molecules to aggregate. When squaraine molecules aggregate in a slip-stacked configuration, the donor and acceptor groups of adjacent squaraine molecules are in close proximity to one another.[17] This is thought to result in a broader absorption spectrum and favorable changes to the morphological characteristics of the active layer, which

[16] Chenyu Zheng, "Spectral Properties of Squaraines and Their Aggregates," MS thesis (Rochester Institute of Technology, 2015): 5.
[17] Soumya Gupta, "Aggregation as an Efficiency Driver in Bulk Heterojunction Devices Measured Through Mixed Squaraines in Ternary Blends," MS thesis (Rochester Institute of Technology, 2020): 16.

governs the transport and dissociation of excitons. However, Zheng and others suggest that aggregation serves to inhibit performance and power-conversion efficiency in squaraine-based organic solar cells in a paper titled "Phase Separation, Crystallinity and Monomer-Aggregate Population Control in Solution Processed Small Molecule Solar Cells." In some cases, the authors suggest, squaraine aggregates will exhibit absorption features where there is no observable fluorescence.[18] Despite being similar molecules, DBSQ(OH)2 and DHSQ(OH)2 blend differently with PCBM. This can be seen in the monochromator absorbance spectra in figure 5, taken by Tyler Wiegand at RIT.

[18] Zheng, et. al. "Phase Separation, Crystallinity and Monomer-Aggregate Population Control in Solution Processed Small Molecule Solar Cells," *Solar Energy Materials and Solar Cells 157* (December 2016): 366.

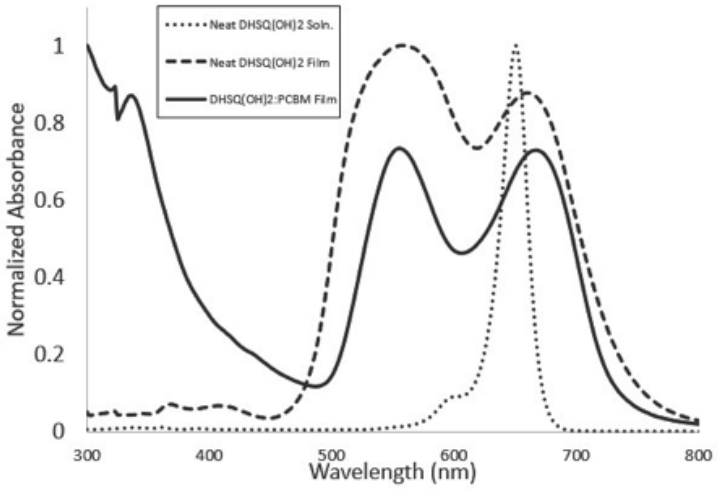

Figure 5: DHSQ:PCBM film absorbance spectrum, taken by Tyler Wiegand.

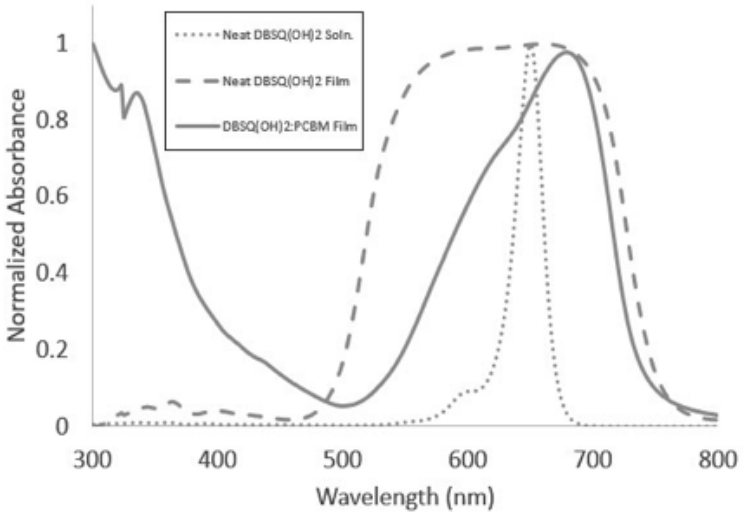

Figure 6: DBSQ:PCBM film absorbance spectrum, taken by Tyler Wiegand.

It is worth noting that the absorbance spectrum of DBSQ is more monomer-like than the double-hump absorption features in the DHSQ spectrum. The DHSQ spectrum suggests poor blending with PCBM.

Methods

PeakForce KPFM

Bruker's *PeakForce* Kelvin Probe Force Microscopy (KPFM) is a scanning probe microscopy technique that allows for nanoscale images of a sample's surface potential and topographical features. High-resolution micrographs obtained with *PeakForce* KPFM provide key insights into the physics of organic semiconductor blends. Because of the important role these images play in our analysis of candidate OPV materials, thorough discussion of the technique and its limitations is necessary to understand and contextualize the results. However, before discussing *PeakForce* KPFM, we believe it is important to familiarize the reader with the atomic force microscopy (AFM) technology it is based on.

To generate an AFM image of a sample, a scan tip mounted on the end of a cantilever beam is introduced to the sample surface. A laser beam is reflected off the back of the cantilever and onto a four-quadrant photodiode. The beam's position on the photodiode is deflected by the movement of the tip-cantilever assembly. The degree to which the scan tip makes contact with the surface depends on the mode of operation that the user has selected. In *contact mode*, the AFM tip is dragged in a raster-scan pattern across the sample. The tip-sample separation is typically less than 0.5 nm in contact mode, resulting in a strong repulsive force between the tip and the sample which, in turn, causes a

deflection of the cantilever.[19] In *non-contact* or *intermediate* (tapping) modes, the cantilever is oscillated vertically at its resonant frequency. The relative strength of the interaction between the tip and sample varies as a function of distance between the two. This variation in tip-sample distance causes a change in the amplitude of oscillation and resonant frequency. These changes in the oscillation amplitude or resonant frequency are monitored and used in a feedback loop to maintain a constant setpoint amplitude, and the motion required to maintain this amplitude is used to extract information about the topography of the sample.

In KPFM-based techniques, the feedback loop uses the cantilever's oscillation amplitude and phase of in response to a force whose strength is governed by backing DC and AC voltages applied between the AFM probe and the sample. The amplitude and phase of the cantilever's oscillation are detected by using a lock-in amplifier. This information is used to extract the relative height of the AFM tip as well as the contact potential difference. Changes in AFM tip height relative to the sample surface are used in a PID controller that recalculates the required tip height to keep the tip-sample separation as constant as possible. Changes in contact potential difference are used to recalculate the required DC bias voltage to compensate for the electrostatic forces between the tip and sample and maintain a closed-loop system.[20]

---

[19] Melitz, et. al. "Kelvin Probe Force Microscopy and Its Application." *Surface Science Reports 66* (2011): 2.
[20] Kilpatrick, et. al. "Quantitative Comparison of Closed-Loop and Dual Harmonic Kelvin Probe Force Microscopy Techniques," *Review of Scientific Instruments 89* (2018): 1.

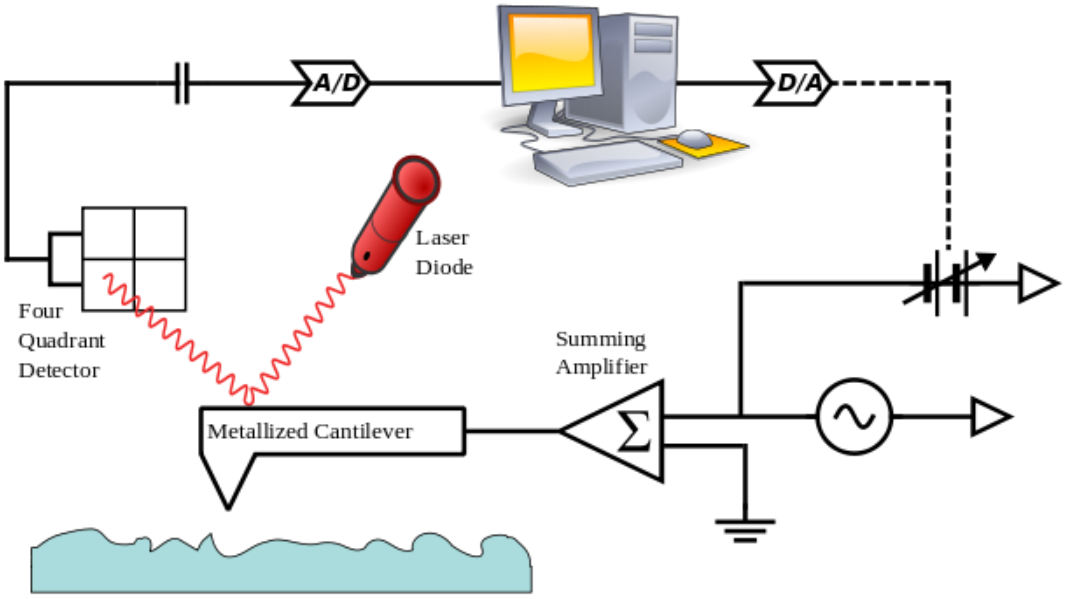

Figure 7: Experimental setup for KPFM.[21]

FM-KPFM is a non-contact variant of AFM used for obtaining high-resolution measurements of surface potential. The oscillating scan tip and the sample surface form two plates of a parallel-plate capacitor.[22] This causes an electrostatic force to act on the cantilever. This force is given by Equation 1, and is proportional to the derivative of the tip-sample capacitance with respect to lift height and the square of the potential difference between the tip and sample.[23]

$$F_{el} = \frac{-1}{2}(dC/dZ)\ (\Delta V)^2 \qquad (1)$$

[21] Inkwina, "Kelvin Probe Force Microscopy." *Wikimedia Commons,* March 1 2008. https://commons.wikimedia.org/wiki/File:Kelvin_probe_force_microscopy.svg
[22] Nonnenmacher, et. al. "Kelvin Probe Force Microscopy," *Applied Physics Letters 58 (1991): 2921.*
[23] Coffey, et. al. "Nanoscale Characterization of Squaraine-Fullerene-Based Photovoltaic Active Layers by Atomic Force Microscopy Mechanical and Electrical Property Mapping," *Thin Solid Films* 669 (2019): 120.

This electrostatic force on the cantilever vanishes when an equal and opposite backing potential is applied to the scan tip. However, in the presence of a changing electric field, the oscillating cantilever will experience a change to its spring constant and resonant frequency given by Equation 2.

$$\Delta\omega \approx -\frac{\omega}{2k}\left(\frac{dF_{el}}{dz}\right) \quad (2)$$

These slight changes in resonant frequency are monitored and used to extract information about the local surface potential at every given point in the scan. To obtain both surface potential and topographical information, intermediate mode (tapping) AFM and FM-KPFM are combined in Bruker's *PeakForce* KPFM mode. To minimize the interference caused by the tapping mode, *PeakForce* KPFM is implemented in a dual-pass configuration: the probe completes one scan laterally in one direction in tapping mode (the trace) and repeats the scan in the reverse direction (the re-trace). Once finished, the process is repeated on the same row in lift mode.

One key advantage of the *PeakForce KPFM* scan mode is its spatial resolution. Ultimately, the spatial resolution of an image formed by a PeakForce KPFM scan is limited by the radius of the probe used. The electromagnetic interaction between a KFPM probe and a sample surface can be modelled using a sphere-plane approximation. One such probe model, described by Li and others

in a technical report for the Bruker Corporation, found that *PeakForce KPFM* is capable of resolving surface potential and topographical features as little as 10 nm apart at a lift height of 5 nm.[24] This makes PeakForce KPFM a powerful tool for imaging domains at the nanoscale. However, because KPFM measurements are relative contact potential differences rather than absolute work functions, we needed to calibrate our PFQNE-AL probes whenever we needed to know the absolute value of the work function. To do this, we took multiple images of the calibration sample provided by Bruker (example image shown in fig. 8). The calibration sample is a silicon substrate patterned with gold and aluminum. In figure 8, gold is on the left hand side and aluminum is on the right, with a smaller strip of silicon separating them. Because the work functions of Al (~4.1 eV) and Au (~5.1 eV) are well-known, we can use the measured contact potential difference between the tip and sample as shown in figure 8 to infer the actual work functions of our samples. Bruker's Analysis software was used to find the average contact potential difference between the tip and sample for the regions of aluminum and gold in each calibration image. This yielded a constant offset which, when applied to KPFM images, would convert the relative contact potential differences into absolute work functions for each sample.

[24] Li, et. al. "Application Note #140," *Bruker Corporation* (2013): 3. Accessed December 9 2020.

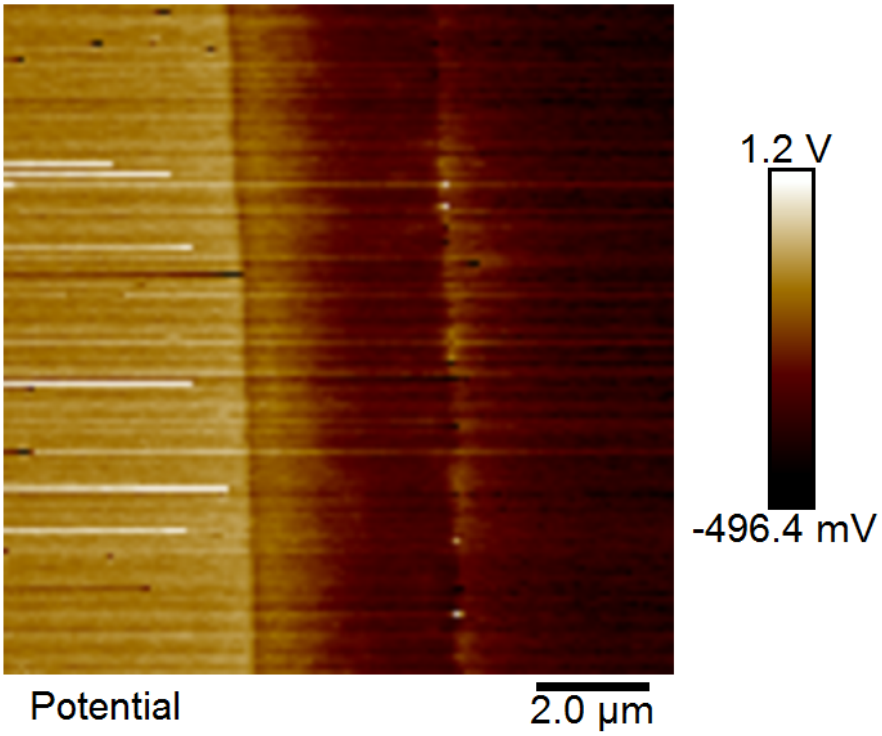

Figure 8: Probe calibration KPFM image. Au left (5.1 eV), Al right (4.1 eV).

We performed the calibration shown in figure 8 regularly whenever the true value of the work function was necessary. The contact potential difference between tip and sample varied with each tip change, and when material from the sample accrued on the tip. In other words, we performed a calibration whenever we were interested in the absolute work function and not the relative contrast within the image. This was done to determine whether or not the DBSQ and DHSQ squaraines had different work function values.

Results and Discussion

Using *PeakForce* KPFM, we imaged various ternary, binary, and pure blends of PCBM and two squaraines: DBSQ(OH)2, and DHSQ(OH)2. In almost all cases, the relative difference in surface potential between materials allows for sufficient contrast to distinguish individual compositional domains. However, because the work functions of DBSQ and DHSQ are very similar, distinguishing between the DBSQ domains and DHSQ domains in a ternary blend is not feasible. The effects of annealing on the crystallinity, domain size, and overall device performance of organic photovoltaic materials are worth noting. First, we will discuss the pure blends, followed by the binary (two-compound) and lastly, the ternary (three-compound) blends.

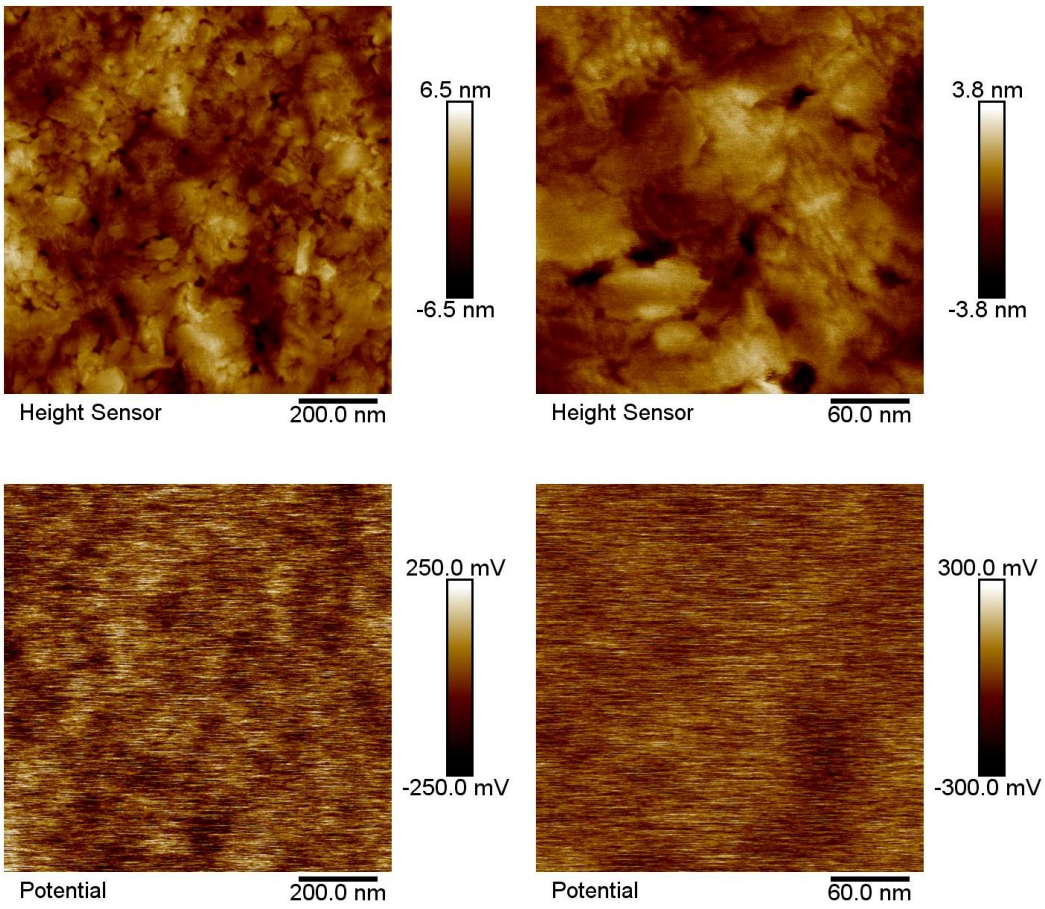

Figure 9: Pure DBSQ(OH)2, unannealed.

Regions of relative high and low surface potential regions are clearly present in the pure DBSQ(OH)2 sample. However, unlike in the binary or ternary blends, these regions are not compositional domains, but rather, regions of varying crystallinity. A correlation analysis between height and surface potential, performed by Dr. Chris Thaxton, found no correlation between the two variables.

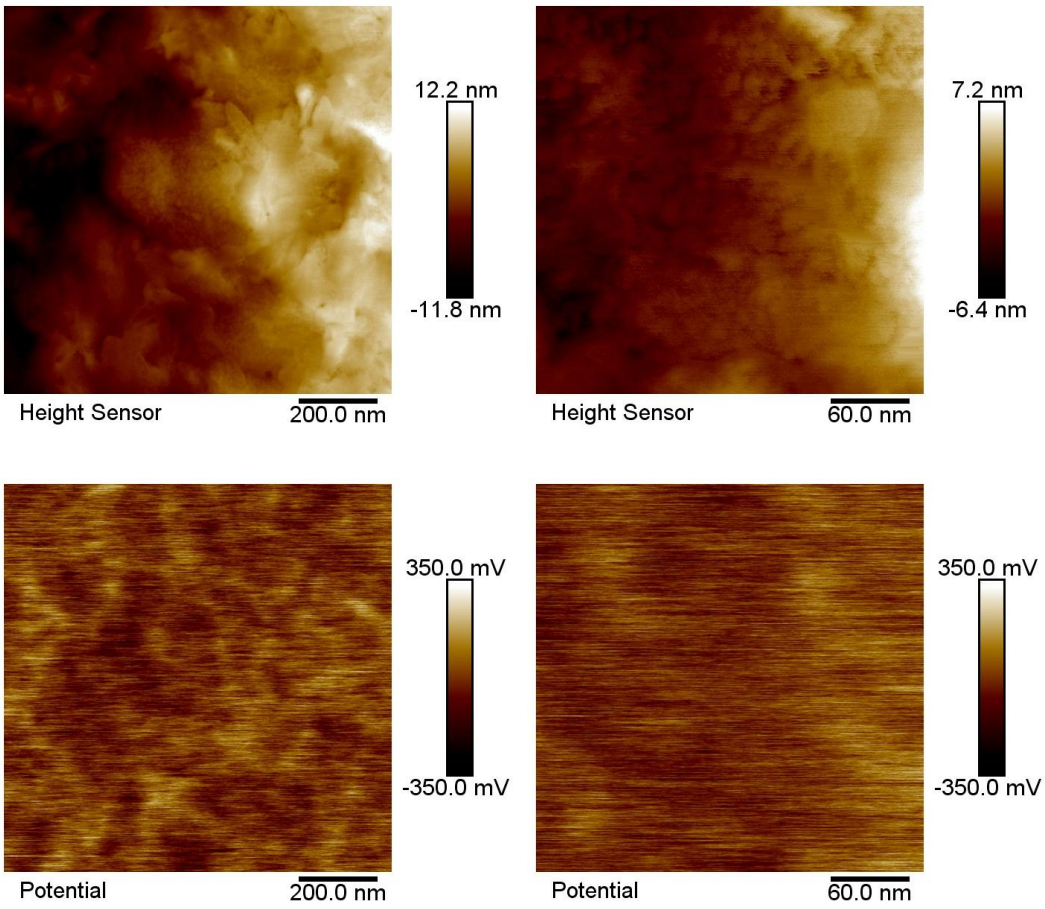

Figure 10: Pure DBSQ(OH)2, annealed at 90°C for 5 minutes.

Compared to the un-annealed sample, the regions in the pure DBSQ(OH)2 are significantly larger, and the KPFM contrast has increased by 100 mV. This annealing-induced increase in contrast can be explained by a well-known phenomenon known as phase separation, in which molecules of the same phase will group preferentially with each other in the presence of thermal annealing.[25]

[25] Wei, et. al. "Annealing-Induced Phase Separation in Small-Molecular Bulk Heterojunctions," *Organic Electronics* 15 (2014): 2810.

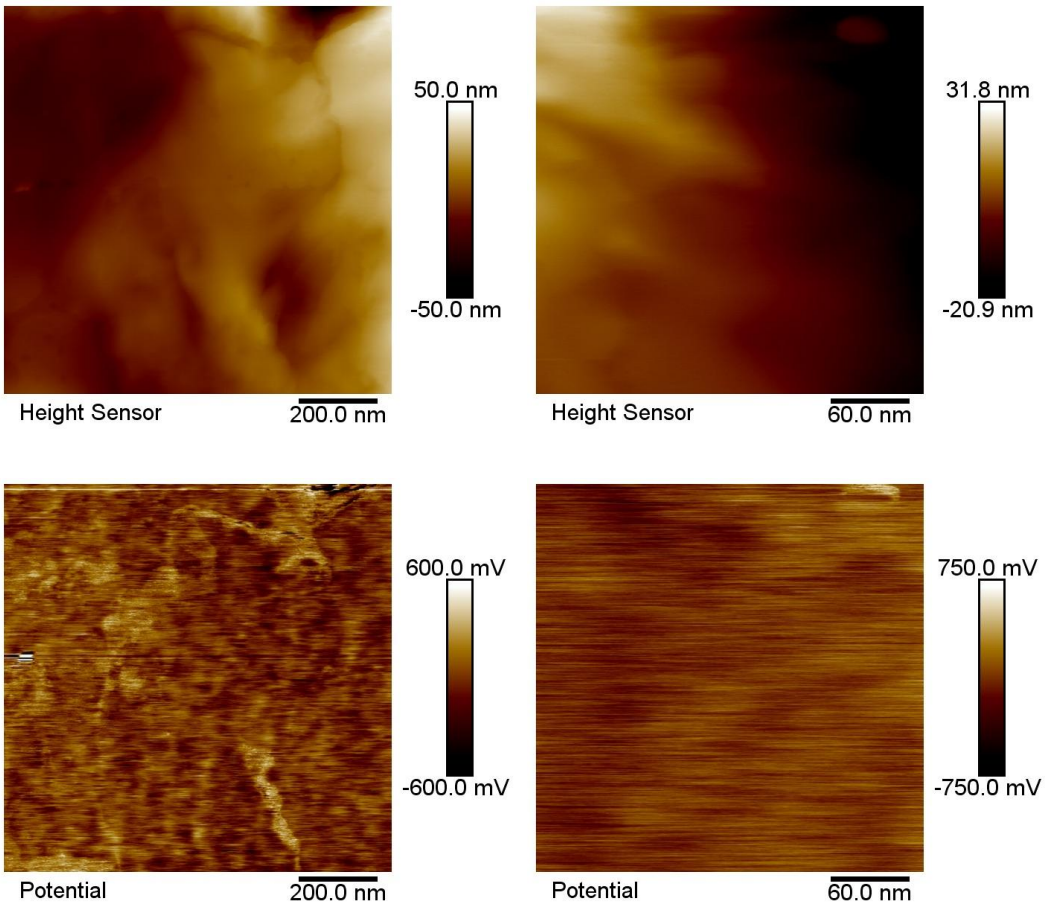

Figure 11: Pure DHSQ(OH)2, unannealed.

The KPFM contrast of pure DHSQ(OH)2 is more than twice that of its pure DBSQ(OH)2 counterpart. The domains also appear to be smaller. A correlation analysis reveals a slight positive correlation between height and surface potential, (m = 0.0897) possibly implying relatively high potential phases collecting at higher topographical locations and vice versa.

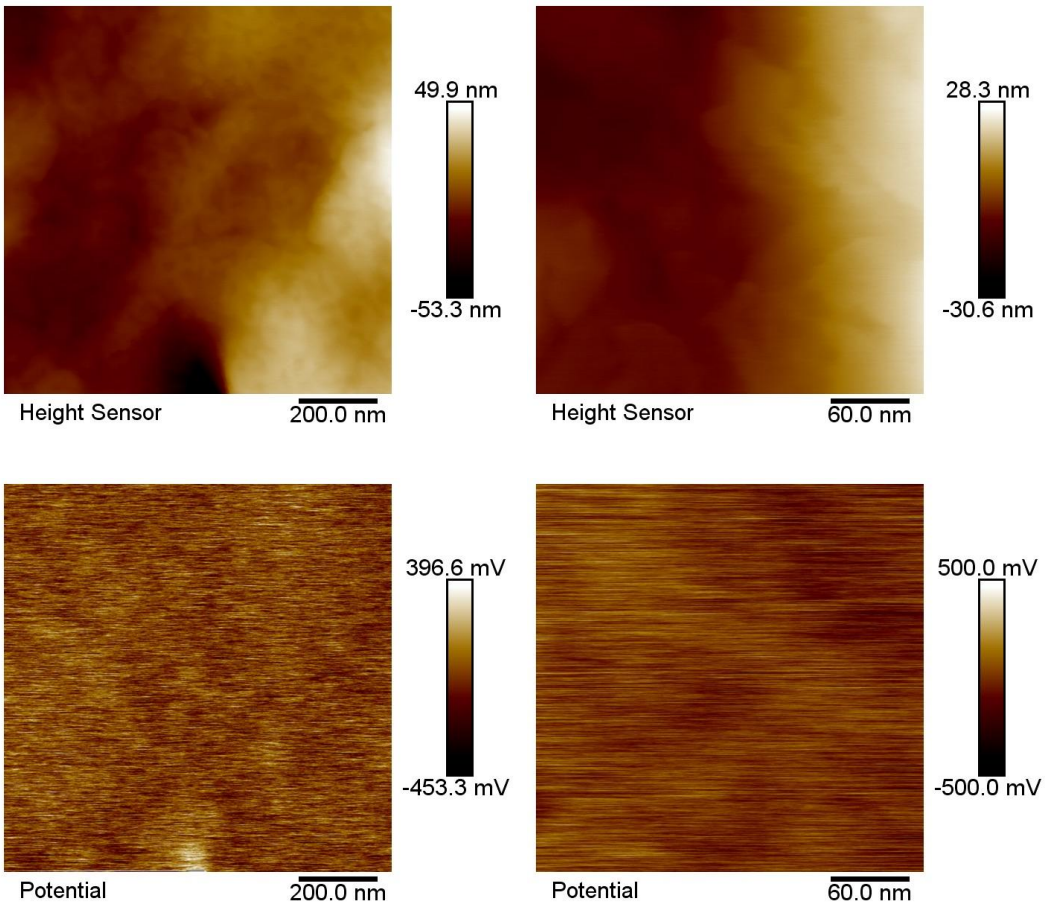

Figure 12: Pure DHSQ(OH)2, annealed at 90°C for 5 minutes.

The crystalline domains in the annealed DHSQ(OH)2 are significantly larger than those in the unannealed DHSQ(OH)2. Unlike every other annealed sample, the KPFM contrast of pure DHSQ(OH)2 decreases when annealed. The height and surface potential appear to be positively correlated with m = 0.1174.

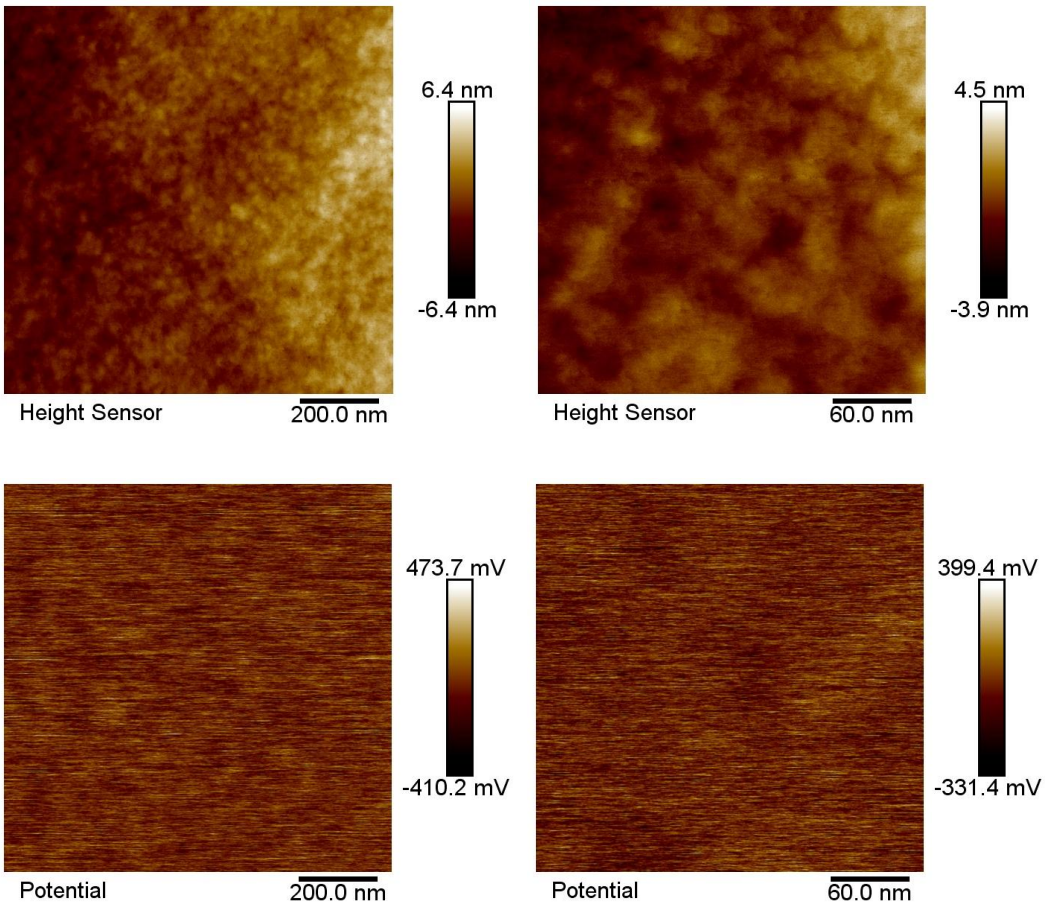

Figure 13: 50:50 blend of DBSQ(OH)2 + PCBM, unannealed.

The annealed (fig. 14) 50:50 blend of DBSQ(OH)2 and PCBM shows remarkable growth in compositional domain sizes compared to its finely-blended unannealed (fig. 13) counterpart.

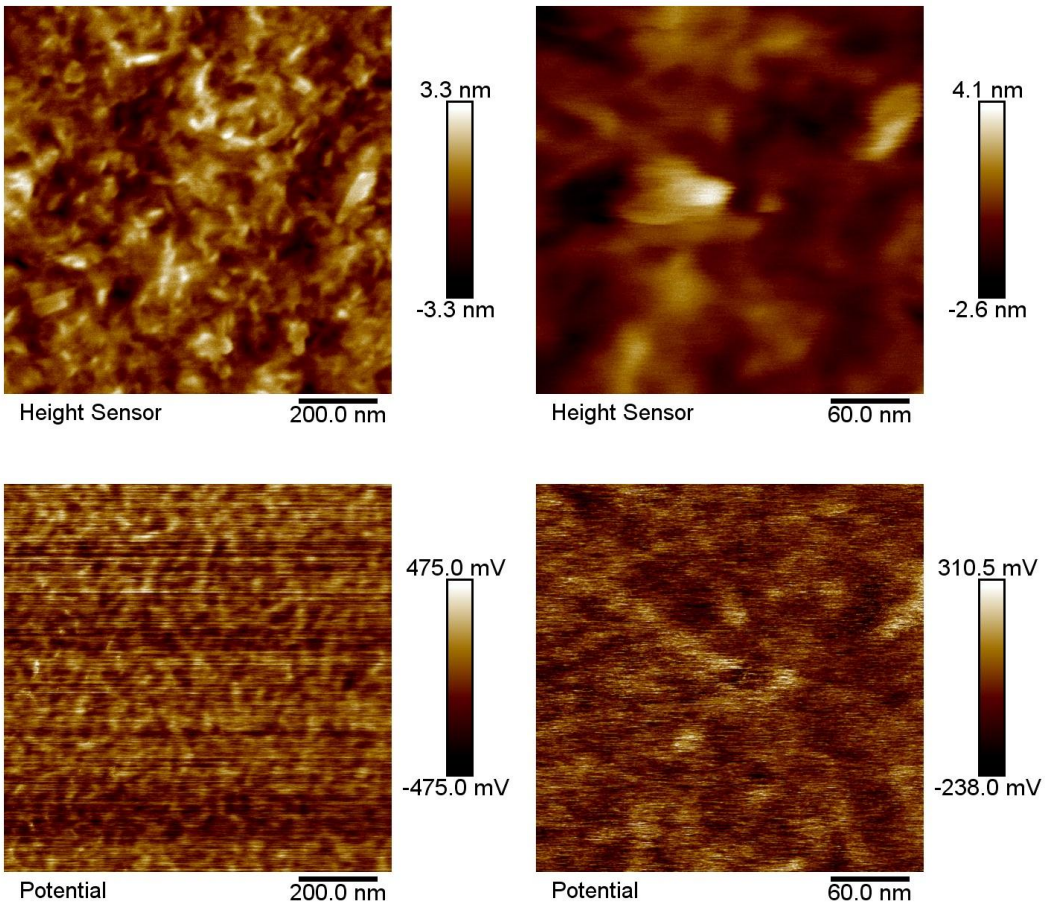

Figure 14: 50:50 blend of DBSQ(OH)2 + PCBM, annealed at 90°C for 5 minutes.

The annealed 50:50 DBSQ:PCBM shows a moderate increase in KPFM contrast compared to its unannealed counterpart. As with the other samples, we believe this is due to like phases aggregating with each other preferentially.

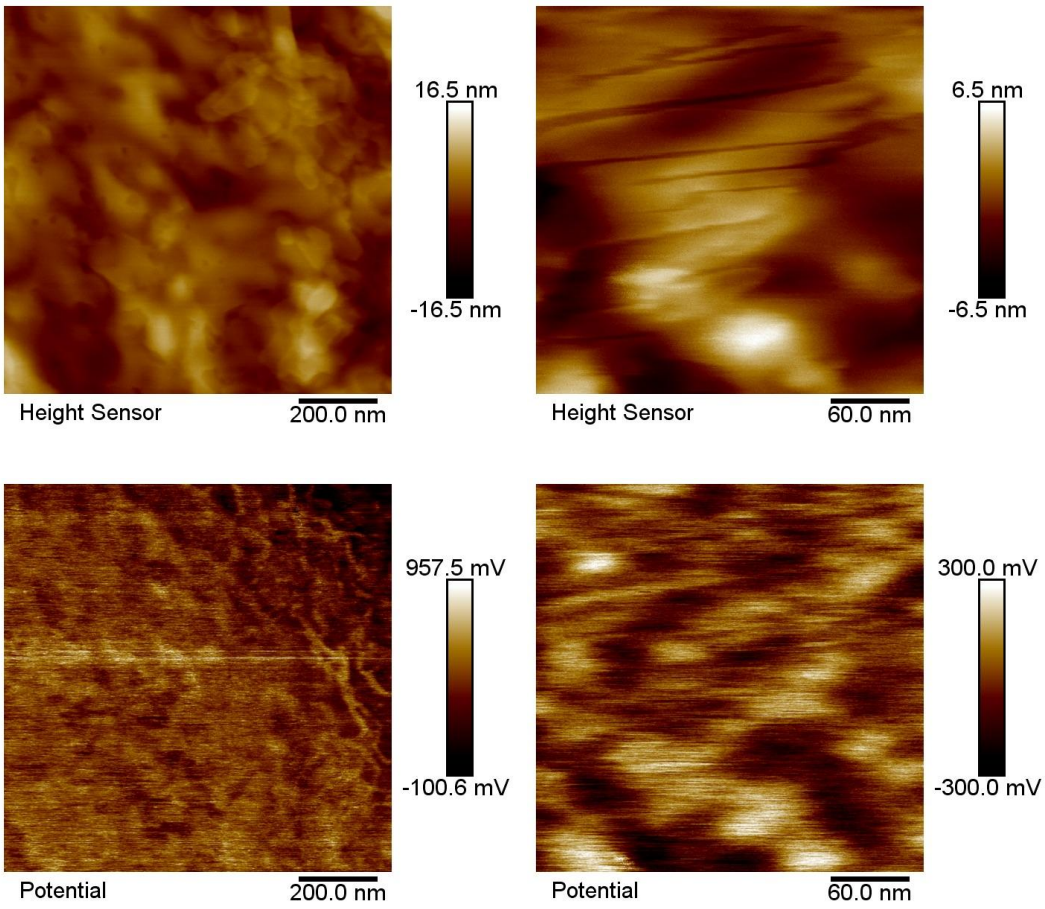

Figure 15: 50:50 blend of DHSQ(OH)2 + PCBM, unannealed.

It is worth noting that in both the annealed and unannealed cases, the compositional domains observed in the DBSQ(OH)2:PCBM blend are much smaller than those observed in the DHSQ(OH)2:PCBM blend. These results agree with the monochromator absorbance spectra in figures 5 and 6 which suggest that DBSQ(OH)2 would blend more readily with PCBM than DHSQ(OH)2.

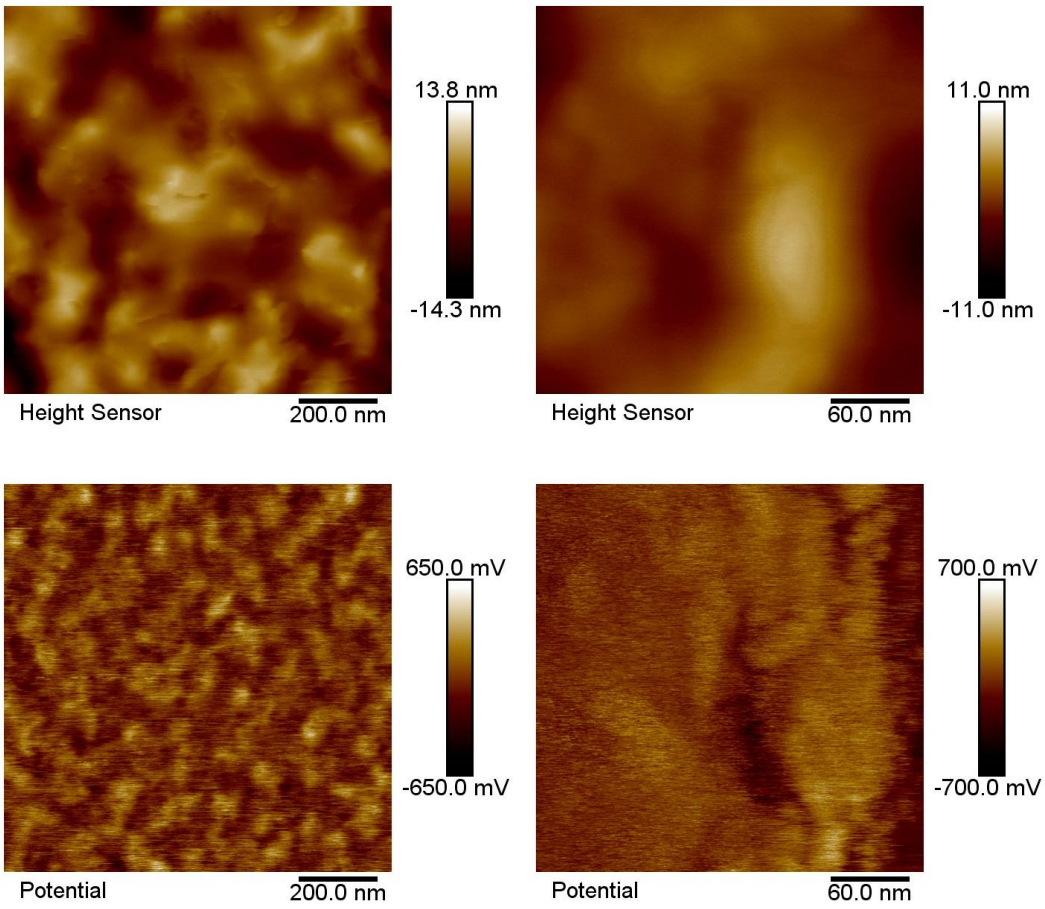

Figure 16: 50:50 blend of DHSQ(OH)2 + PCBM, annealed at 90°C for 5 min.

The domains in the annealed 50:50 DHSQ(OH)2:PCBM sample are much larger than those in the unannealed blend, and the KPFM contrast is more than twice that of the unannealed 50:50 blend. We believe this is due to annealing-induced phase separation in the sample.

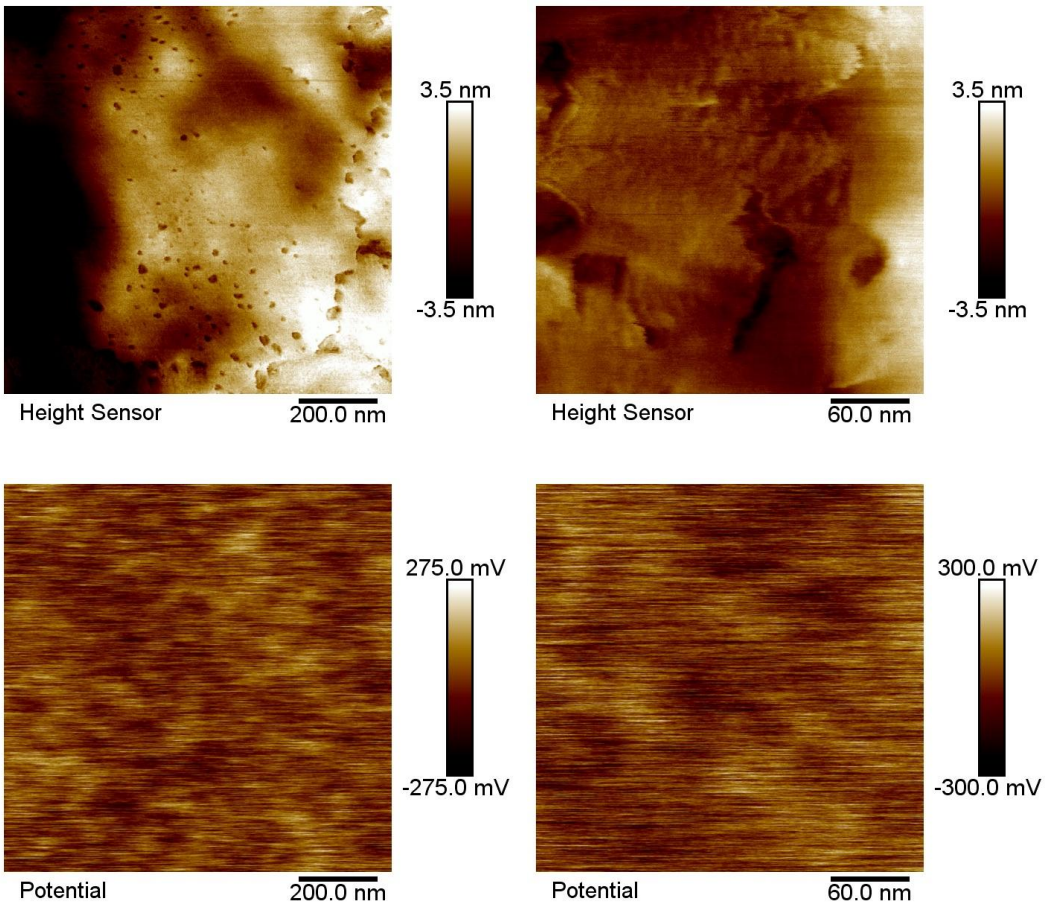

Figure 17: 50:50 blend of DBSQ(OH)2 + DHSQ(OH)2, unannealed.

Because both squaraines have indistinguishable work functions, this image does not provide any information about the blending of the materials. Instead, we believe the local variations in surface potential to be due to varying crystallinity in the sample.

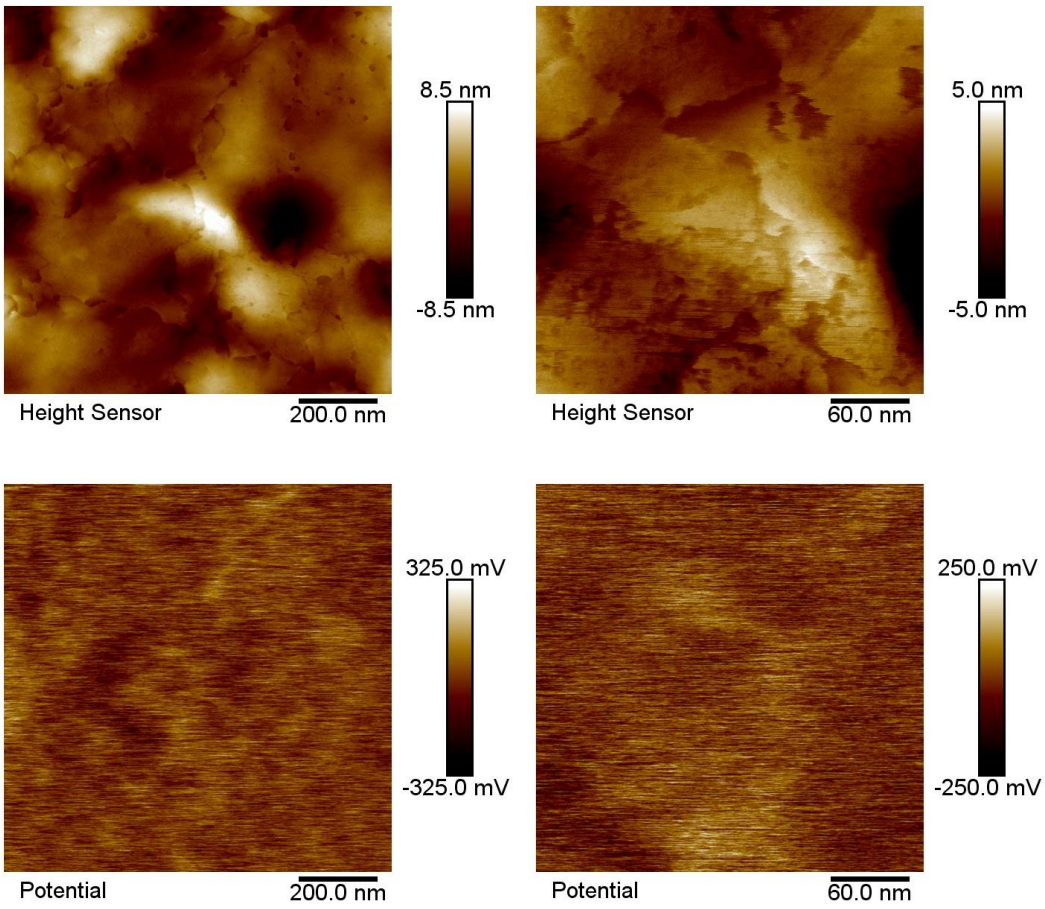

Figure 18: 50:50 blend of DBSQ(OH)2 + DHSQ(OH)2, annealed at 90°C for 5 minutes.

There is a slight increase in contrast and surface roughness in the annealed 50:50 DBSQ:DHSQ sample. The regions of varying surface potential appear to have coalesced and grown larger.

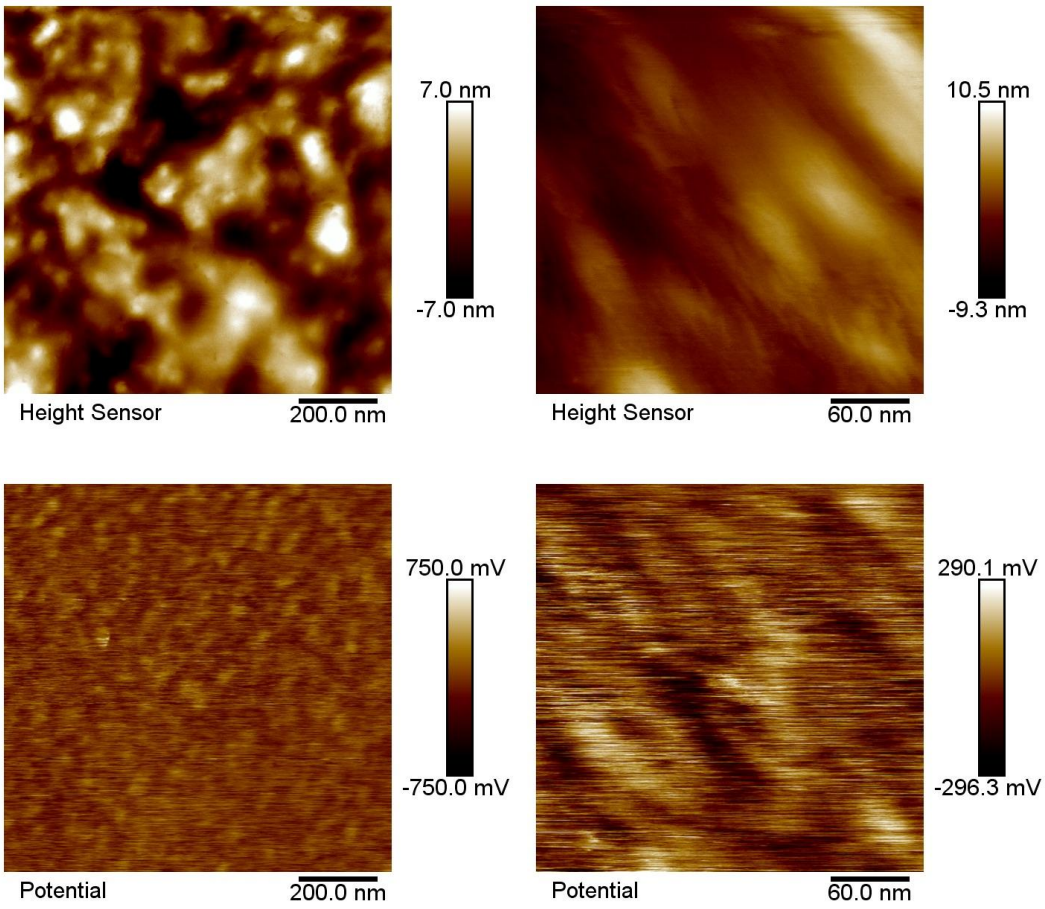

Figure 19: 50:10:40 blend of PCBM + DBSQ(OH)2 + DHSQ(OH)2, unannealed.

One challenge associated with assessing images of ternary blends is the inability to distinguish between compositional domains of DBSQ(OH)2 and DHSQ(OH)2. As we saw in our calibration image, both materials have average work functions of 4.5-4.6 eV, and so they will be indistinguishable in a KPFM image.

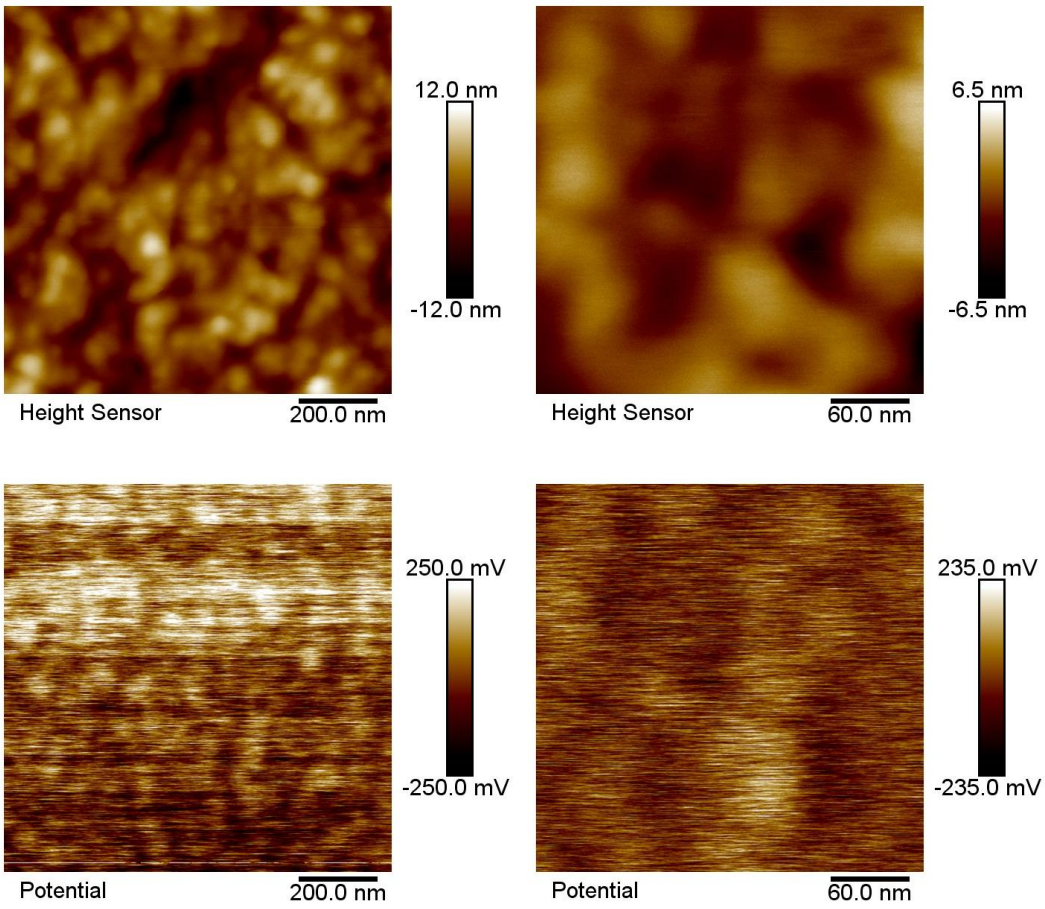

Figure 20: 50:10:40 blend of PCBM + DBSQ(OH)2 + DHSQ(OH)2, annealed at 90°C for 5 minutes.

This sample experienced a slight decrease in surface roughness when annealed. The unannealed sample (fig. 19) had an RMS surface roughness of 0.0959, compared to the annealed sample's RMS surface roughness of 0.0672.

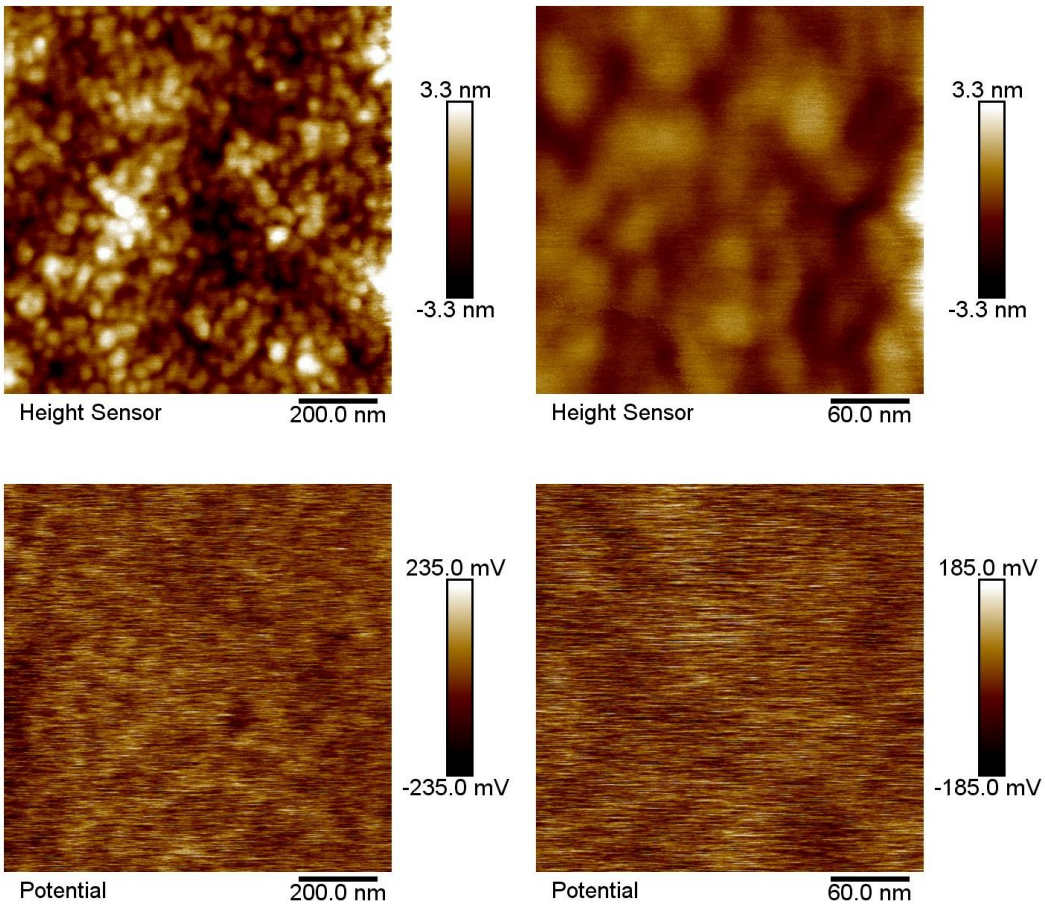

Figure 21: 50:40:10 blend of PCBM + DBSQ(OH)2 + DHSQ(OH)2, unannealed.

This ternary blend appears to have much smaller compositional domains than the binary DBSQ:PCBM or DHSQ:PCBM blends.

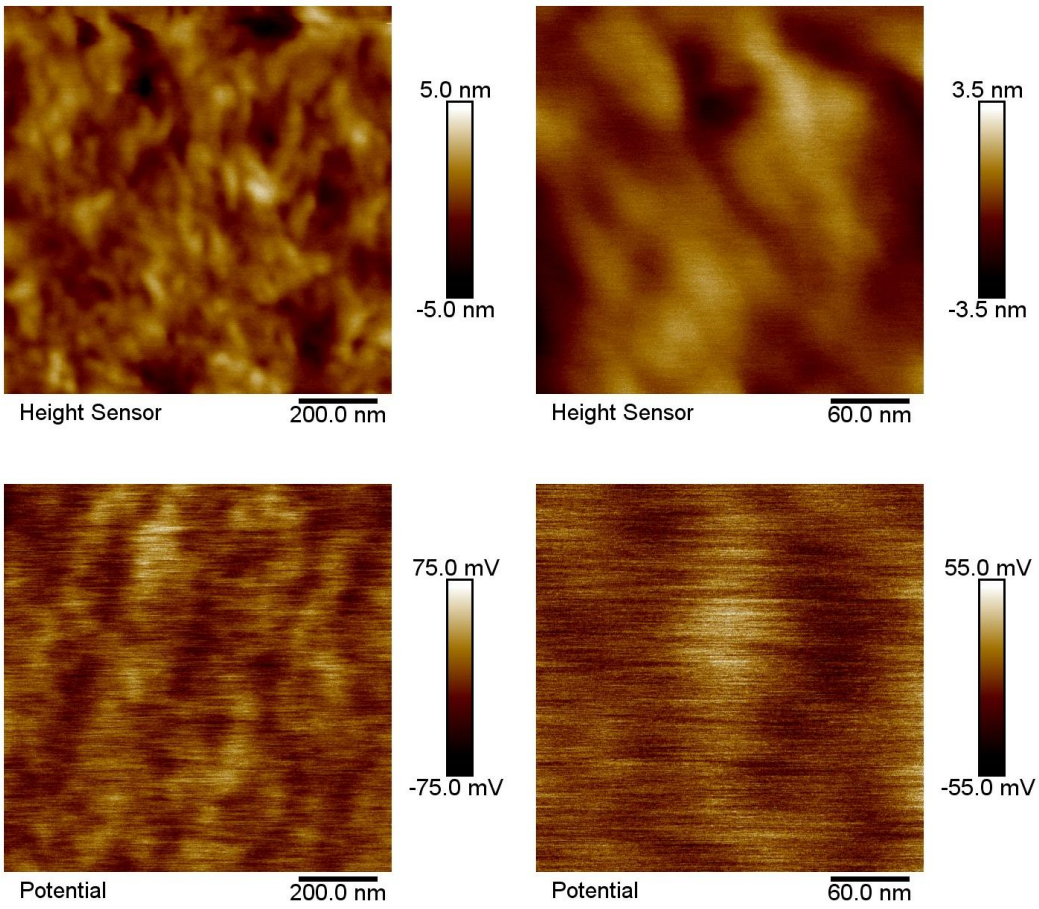

Figure 22: 50:40:10 blend of PCBM + DBSQ(OH)2 + DHSQ(OH)2, annealed at 90°C for 5 minutes.

The annealed 50:40:10 PCBM:DBSQ:DHSQ blend had the lowest KPFM contrast of the samples we imaged. The root-mean-square roughness of the annealed sample was 0.0166, roughly a five-fold decrease from the unannealed sample's RMS roughness of 0.0561. The compositional domains also appear to have elongated.

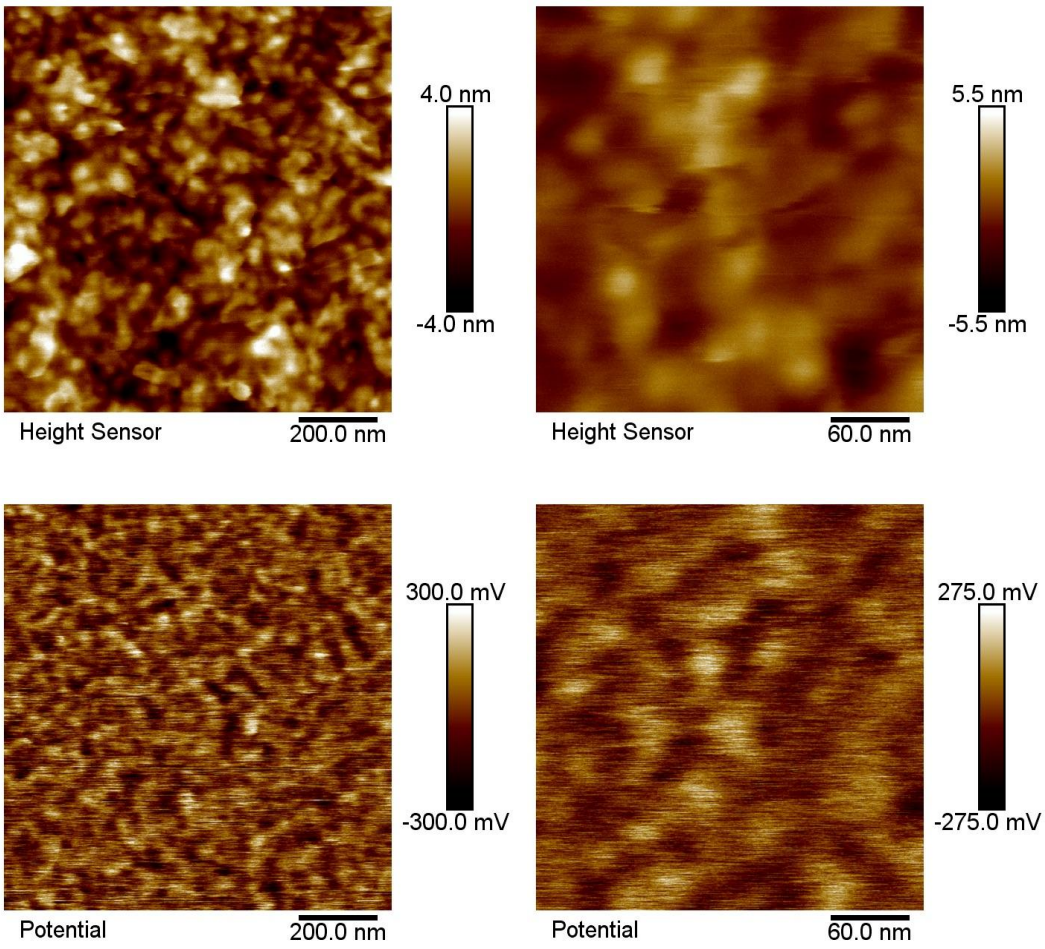

Figure 23: 50:25:25 blend of PCBM + DBSQ(OH)2 + DHSQ(OH)2, unannealed.

This blend appears to have much smaller compositional domains than the binary PCBM:DBSQ and PCBM:DHSQ samples.

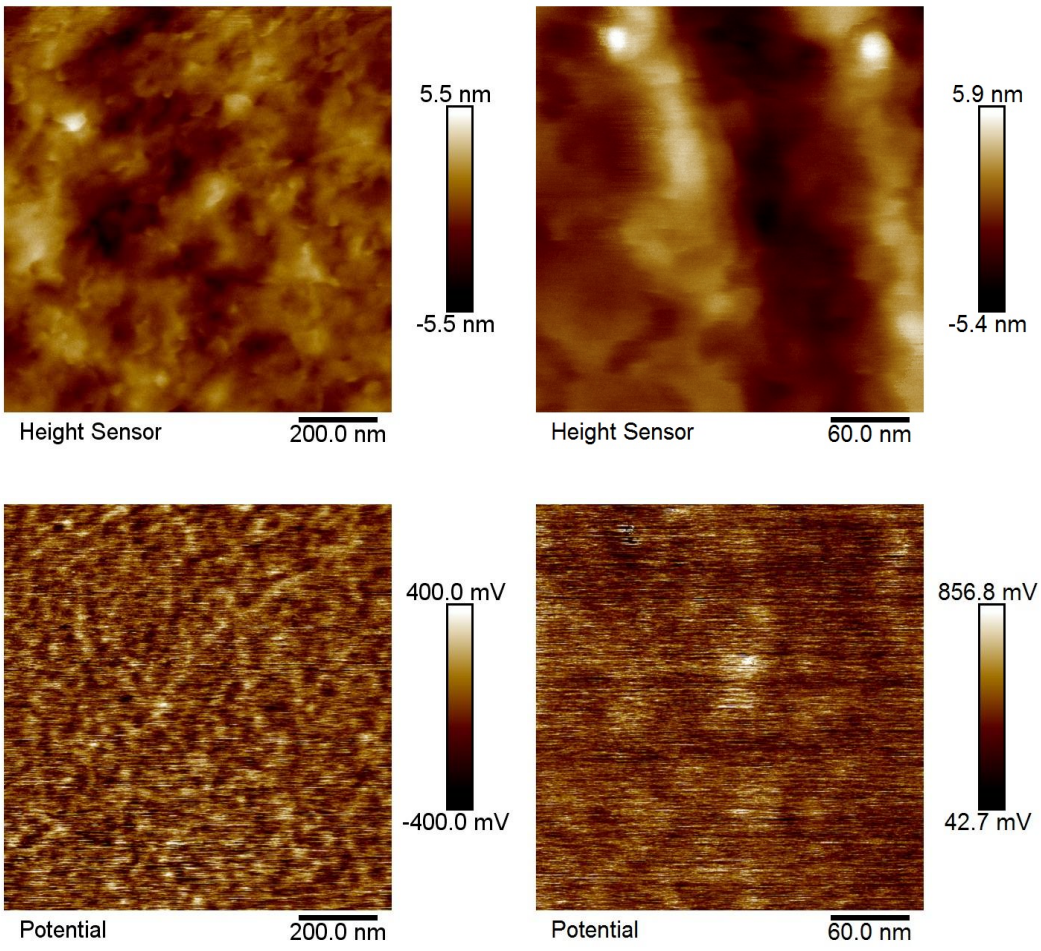

Figure 24: 50:25:25 blend of PCBM + DBSQ(OH)2 + DHSQ(OH)2, annealed at 90°C for 5 minutes.

The 50:25:25 PCBM:DBSQ:DHSQ sample had the smallest surface potential domains. After annealing, the KFPM contrast increased by a total of 200 mV.

Table 1: KPFM mean value, average roughness, and RMS roughness by sample. Analysis courtesy of Dr. Chris Thaxton at Appalachian State University.

Compound Name	Annealing	KPRM: Mean (V)	KPFM: RA (V)	KPFM: RQ (V)
PCBM : DBSQ(OH)2	No	0.454701	0.0993	0.0787
PCBM : DBSQ(OH)2 : DHSQ(OH)2 (50:10:40)	No	0.478355	0.121	0.0959
PCBM : DBSQ(OH)2 : DHSQ(OH)2 (50:10:40)	90°C, 5 min	-0.025683	0.0841	0.0672
PCBM : DBSQ(OH)2 : DHSQ(OH)2 (50:40:10)	No	0.21043	0.0708	0.0561
PCBM : DBSQ(OH)2 : DHSQ(OH)2 (50:40:10)	90°C, 5 min	0.354583	0.0208	0.0166
DBSQ(OH)2 : DHSQ(OH)2 (50:50)	No	0.359806	0.073	0.0581
DBSQ(OH)2 : DHSQ(OH)2 (50:50)	90°C, 5 min	0.410197	0.0702	0.0559
DBSQ(OH)2	No	0.333739	0.0965	0.0768
DBSQ(OH)2	90°C, 5 min	0.120857	0.0849	0.0675
DHSQ(OH)2	No	0.393168	0.0957	0.0751
DHSQ(OH)2	90°C, 5 min	0.267232	0.108	0.0773
PCBM : DBSQ(OH)2	No	-0.118647	1.37	0.58
PCBM : DBSQ(OH)2	90°C, 5 min	-0.06911	0.0855	0.0674
PCBM : DHSQ(OH)2 : DBSQ(OH)2	No	0.151762	0.113	0.0889
PCBM : DHSQ(OH)2 : DBSQ(OH)2	90°C, 5 min	-0.005824	0.111	0.088
PCBM : DHSQ(OH)2	No	0.203887	0.180	0.143
PCBM : DHSQ(OH)2	90°C, 5 min	0.233363	0.133	0.106

Conclusion

In the previous section, we have presented KPFM data obtained here at Appalachian State University, on samples prepared at the Rochester Institute of Technology. One noteworthy observation we have made is that the two squaraines present in our samples (DBSQ + DHSQ) have very similar work functions. In other words, we cannot distinguish compositional domains of DBSQ and DHSQ present in samples containing both of them using KPFM.

We believe that any contrast in KPFM images of the 50:50 DBSQ/DHSQ samples (figs. 17, 18) as well as in the KPFM images pure DBSQ (figs. 9, 10) or DHSQ (figs. 11, 12) can best be explained as the result of local variations in crystallinity or packing which, in turn, can cause changes in the contact potential difference. In most samples, we also noticed a significant increase in contrast when the samples were annealed. We believe this is due to the tendency of different phases of the same molecule to aggregate preferentially to other molecules of like phase. Our PeakForce KPFM measurements, when combined with our collaborators' monochromator spectra and electrical measurements, can help inform our understanding on the nanoscale structures present in these devices, and how they impact device physics and performance.

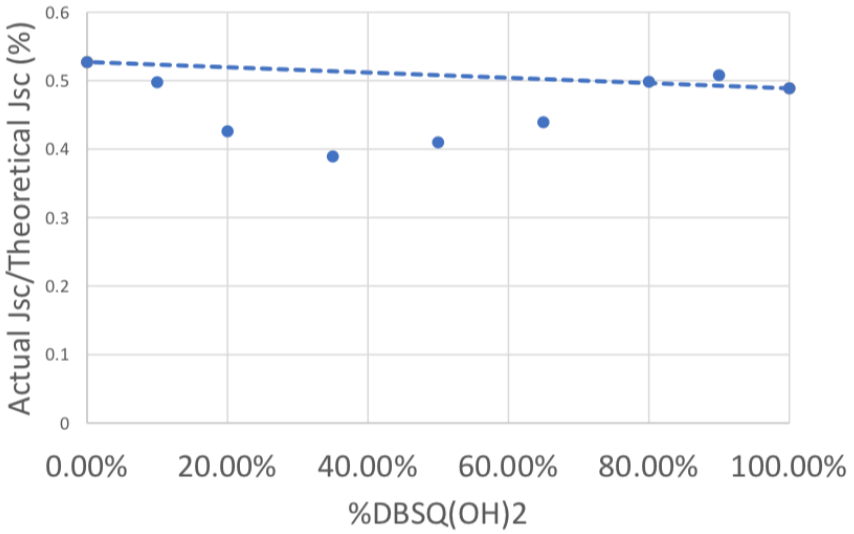

Figure 25: Measured short-circuit current density, normalized with respect to the theoretical short-circuit current density, expressed as a function of the percentage of DBSQ in each blend. Figure courtesy of Tyler Wiegand (RIT).

One useful metric of the performance of a photovoltaic device is the short-circuit current density, which is how much current passes through the device per unit area when no external voltage is being applied to it. This current density is due solely to the charge generation and extraction processes caused by the absorption of light by the device, and so can be used to compare the efficiency of photovoltaic devices. As we have noted in previous sections, DBSQ-like blends tend to have smaller domain sizes, whereas DHSQ-like blends tend to have higher-crystallinity and more tightly packed domains. When blending the two with PCBM in a ternary blend, we found an unexpected dip in short-circuit

current density (and transitively, performance) as the ratio of DBSQ and DHSQ approached 50:50. As we discussed in the background section, smaller domains are thought to dissociate excitons more efficiently, and should in theory result in a larger short-circuit current density when illuminated. Despite having small compositional domains, the 50:25:25 PCBM:DBSQ:DHSQ blend yielded one of the lowest short-circuit current densities when illuminated. We had hoped that blending PCBM with both DBSQ and DHSQ would result in a blend with the highly-crystallized domains of the DHSQ blends and the small domains of the DBSQ blends. However, the KPFM and monochromator data shows that neither the good blending of the DBSQ blends nor the high crystallinity, tightly packed domains of the DHSQ blends are present in the middle-ground 50:25:25 blend.

Bibliography

Bhat, Showkat Ahmad, Tehseen Hassan, and Sabhiya Majid. "Heavy Metal Toxicity and Their Harmful Effects on Living Organisms – a Review." *International Journal of Medical Science And Diagnosis Research* 3 (January 2019): 106–122. https://www.ijmsdr.com/index.php/ijmsdr/article/view/210

Chowdhury, Md. Shahariar, Kazi Sajedur Rahman, Tanjia Chowdhury, Narissara Nuthammachot, Kuaanan Techato, Md. Akhtaruzzaman, Sieh Kiong Tiong, Kamaruzzaman Sopian, and Nowshad Amin. "An Overview of Solar Photovoltaic Panels' End-of-Life Material Recycling." *Energy Strategy Reviews* 27 (January 2020): 1–11. https://doi.org/10.1016/j.esr.2019.100431

Coffey, Tonya, Andrew Seredinski, Jake N. Poler, Crystal Patteson, William H. Watts, Kenny Baptiste, Chenyu Zheng, Jeremy Cody, and Christopher J. Collison. "Nanoscale Characterization of Squaraine-Fullerene-Based Photovoltaic Active Layers by Atomic Force Microscopy Mechanical and Electrical Property Mapping." *Thin Solid Films* 669 (January 2019): 120–32. https://doi.org/10.1016/j.tsf.2018.10.046.

Cubane. "PCBM." *Wikimedia Commons*. November 7, 2009. https://commons.wikimedia.org/wiki/File:PCBM.png

Gupta, Soumya. "Aggregation as an Efficiency Driver in Bulk Heterojunction Devices Measured Through Mixed Squaraines in Ternary Blends." MS thesis. Rochester Institute of Technology, 2020. 84.

Inkwina, "Kelvin Probe Force Microscopy." *Wikimedia Commons*. March 1, 2008. https://commons.wikimedia.org/wiki/File:Kelvin_probe_force_microscopy.svg

International Energy Association, "Global Energy Review 2020." April 30, 2020. https://www.iea.org/reports/global-energy-review-2020

Jacobkhed, "Jablonski diagram of absorbance, non-radiative decay, and fluorescence." *Wikimedia Commons*. April 22 2012. https://commons.wikimedia.org/wiki/File:Jablonski_Diagram_of_Fluorescence_Only.png

Kilpatrick, Jason I., Liam Collins, Stefan A. L. Weber, and Brian J. Rodriguez. "Quantitative Comparison of Closed-Loop and Dual Harmonic Kelvin Probe Force Microscopy Techniques." *Review of Scientific Instruments* 89, no. 12 (December 2018): 123708. https://doi.org/10.1063/1.5025432.

Li, et. al. "Application Note #140." Bruker Corporation, 2013, 3. Accessed December 9 2020. https://bruker.com/fileadmin/user_upload/8-PDF-Docs/SurfaceAnalysis/AFM/ApplicationNotes/AN140-RevA1-PeakForce_KPFM-AppNote.pdf

Liu, Tao, and Alessandro Troisi. "What Makes Fullerene Acceptors Special as Electron Acceptors in Organic Solar Cells and How to Replace Them." *Advanced Materials* 25, no. 7 (February 2013): 1038–41. https://doi.org/10.1002/adma.201203486.

Melitz, Wilhelm, Jian Shen, Andrew C. Kummel, and Sangyeob Lee. "Kelvin Probe Force Microscopy and Its Application." *Surface Science Reports* 66, no. 1 (January 2011): 1–27. https://doi.org/10.1016/j.surfrep.2010.10.001.

Myung-Su Kim. "Understanding Organic Photovoltaic Cells: Electrode, Nanostructure, Reliability, and Performance." PhD dissertation. University of Michigan, 2009: 130. https://deepblue.lib.umich.edu/handle/2027.42/62335

Nonnenmacher, et. al. "Kelvin Probe Force Microscopy." *Applied Physics Letters* 58 (June 1991): 2921–2923. https://doi.org/10.1063/1.105227

Smokefoot. "Trans-CH(n)." *Wikimedia Commons*. December 28 2008. https://commons.wikimedia.org/wiki/File:Trans-(CH)n.png

Spooner, Emma. "Organic Photovoltaics: An Introduction." *Ossila.* Accessed January 25 2021. https://www.ossila.com/pages/organic-photovoltaics-introduction

Su, L.C., H.D. Ruan, D.J. Ballantine, C.H. Lee, and Z.W. Cai. "Release of Metal Pollutants from Corroded and Degraded Thin-Film Solar Panels Extracted by Acids and Buried in Soils." Applied Geochemistry 108 (September 2019): 104381. https://doi.org/10.1016/j.apgeochem.2019.104381

The Royal Swedish Academy of Sciences. "The 2000 Nobel Prize in Chemistry." Oct. 10th, 2000. https://www.nobelprize.org/prizes/chemistry/2000/popular-information/

Tomgally. "Molecule HOMO-LUMO diagram.svg." Wikimedia Commons. January 19, 2020. https://upload.wikimedia.org/wikipedia/commons/7/7b/Molecule_HOMO-LUMO_diagram.svg

Wei, Huai-Xin, Yan-Qing Li, Xiang-Yu Chen, Chun-Sing Lee, and Jian-Xin Tang. "Annealing-Induced Phase Separation in Small-Molecular Bulk Heterojunctions." *Organic Electronics* 15, no. 11 (November 2014): 2810–16. https://doi.org/10.1016/j.orgel.2014.08.017.

World Meteorological Organization, December 2020. "State of the Global Climate 2020: Provisional Report." Accessed December 29 2020. https://public.wmo.int/en/our-mandate/climate/wmo-statement-state-of-global-climate

Yang, Liyan, Shaoqing Zhang, Chang He, Jianqi Zhang, Huifeng Yao, Yang Yang, Yun Zhang, Wenchao Zhao, and Jianhui Hou. "New Wide Band Gap Donor for Efficient Fullerene-Free All-Small-Molecule Organic Solar Cells." *Journal of the American Chemical Society* 139, no. 5 (February 2017): 1958–66. https://doi.org/10.1021/jacs.6b11612.

Zheng, Chenyu. "Spectral Properties of Squaraines and Their Aggregates, Targeted for Use in Bulk Hetero-Junction Solar Cells," MS thesis. Rochester Institute of Technology, 2015: 151. https://scholarworks.rit.edu/theses/8923

Zheng, Chenyu, Dylan Bleier, Ishita Jalan, Sarah Pristash, Anirudh Raju Penmetcha, Nicholas J. Hestand, Frank C. Spano, Michael S. Pierce, Jeremy A. Cody, and Christopher J. Collison. "Phase Separation, Crystallinity and Monomer-Aggregate Population Control in Solution Processed Small Molecule Solar Cells." *Solar Energy Materials and Solar Cells* 157 (December 2016): 366–76. https://doi.org/10.1016/j.solmat.2016.05.060.

Zheng, Chenyu, Ishita Jalan, Patrick Cost, Kyle Oliver, Anju Gupta, Scott Misture, Jeremy A. Cody, and Christopher J. Collison. "Impact of Alkyl Chain Length on Small Molecule Crystallization and Nanomorphology in Squaraine-Based Solution Processed Solar Cells." *The Journal of Physical Chemistry C* 121, no. 14 (April 2017): 7750–60. https://doi.org/10.1021/acs.jpcc.7b01339.

Vita

Joseph P. Godoy was born in Miami, Florida, and raised in Glastonbury, Connecticut. In the fall of 2015, he enrolled at High Point University, where he completed his Bachelor of Science in Physics with a minor in Mathematics in 2019. From 2019 to 2021, he attended Appalachian State University and studied to earn a Master of Science degree in Engineering Physics. He now resides in Winston-Salem.